LANGMUIR Article
Cite This: Langmuir 2018, 34, 5696−5702
pubs.acs.org/Langmuir

Electronic Structure of a Self-Assembled Monolayer with Two Surface Anchors: 6-Mercaptopurine on Au(111)

Cynthia C. Fernández,[†] Evangelina Pensa,[‡] Pilar Carro,[§] Roberto Salvarezza,[‡] and Federico J. Williams*[,†]

[†]Departamento de Química Inorgánica, Analítica y Química Física, Facultad de Ciencias Exactas y Naturales, INQUIMAE-CONICET, Universidad de Buenos Aires, Ciudad Universitaria, Pabellón 2, Buenos Aires C1428EHA, Argentina

[‡]Facultad de Ciencias Exactas, Instituto de Investigaciones Fisicoquímicas Teóricas y Aplicadas (INIFTA), Universidad Nacional de La Plata, CONICET, La Plata 1900, Argentina

[§]Área de Química Física, Departamento de Química, Facultad de Ciencias, Universidad de La Laguna, Instituto de Materiales y Nanotecnología, Avda. Francisco Sánchez, s/n, 38200 La Laguna, Tenerife, Spain

ABSTRACT: The electronic structure of aromatic and aliphatic thiols on Au(111) has been extensively studied in relation to possible applications in molecular electronics. In this work, the effect on the electronic structure of an additional anchor to the S−Au bond using 6-mercaptopurine as a model system has been investigated. Results from X-ray photoelectron spectroscopy, near-edge X-ray absorption fine structure spectroscopy, and density functional theory (DFT) confirm that this molecule adsorbs on Au(111) with S−Au and iminic N−Au bonds. Combined ultraviolet photoelectron spectroscopy and DFT data reveal that formation of the 6MP self-assembled monolayer generates a molecular dipole perpendicular to the surface, with negative charges residing at the metal/monolayer interface and positive charges at the monolayer/vacuum interface, which lowers the substrate work function. Scanning tunneling microscopy shows two surface molecular domains: a well-ordered rectangular lattice where molecules are tilted on average 30° with respect to the substrate and aligned 6MP islands where molecules are standing upright. Finally, we found a new electronic state located at −1.7 eV with respect to the Fermi level that corresponds to a localized π molecular state, while the state corresponding to the N−Au bond is hybridized with Au d electrons and stabilized at much lower energies (−3 eV).

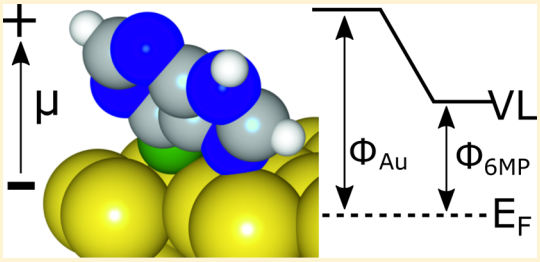

INTRODUCTION

Purines are heterocyclic compounds consisting of an imidazole ring fused with a pyrimidine ring. These aromatic molecules are present in diverse biological systems and take part in the core structure of guanine and adenine. One of the most important purines is 6-mercaptopurine (6MP), a synthetic nitrogen containing heterocyclic thiol that is very effective for the treatment of leukemia, autoimmune disorders, and other diseases.[1,2]

The adsorption of 6MP on solid substrates have attracted considerable attention because some of the problems found in the pharmacological treatment could be circumvent using 6MP-functionalized nanoparticles as carriers.[3−5] As a consequence, the structural properties of 6MP over solid surfaces were studied over the past years. 6MP chemisorbs strongly on Au surfaces after the formation of S−Au thiolate and iminic N−Au bonds, that is, it forms a double anchor to Au substrates.[6] The molecule self-assembles on Au(111) single crystal surfaces, lifting the substrate reconstruction.[7] Interestingly, these ordered structures do not contain staple moieties (RS−Au_{ad}−SR), which are a proposed adsorption model for thiol-based self-assembled monolayers (SAMs).[8] Chemisorption of the molecule on Au(111) yields short-range ordered two-dimensional (2D) lattices, whereas chemisorption on Au(001) results in long-range well-ordered SAMs.[9] 6MP molecules bind to silver surfaces with a tilted molecular plane,[10,11] whereas they adsorb with a flat lying geometry over graphene layers.[12] Vibrational spectroscopic measurements suggest that 6MP molecules bind on Au surfaces with the molecular plane standing upright.[13] Although the molecular structure of the adsorbate has been studied on different substrates, its electronic structure has only been measured on graphene surfaces using photoemission spectroscopy.[12] Furthermore, little is known about the electronic structure of thiol SAMs with an additional N−Au interaction. Thus, the study of the electronic density of states (DOS) of 6MP on Au is both relevant and interesting.

In this work, we present a detailed study of the valence electronic structure of 6MP SAMs on Au(111) surfaces. New insights arise from the combination of photoemission measurements and density functional theory (DFT) calculations. Furthermore, near-edge X-ray absorption fine structure spectroscopy (NEXAFS) and scanning tunneling microscopy (STM) measurements combined with DFT calculations

Received: March 11, 2018
Revised: April 27, 2018
Published: May 1, 2018

DOI: 10.1021/acs.langmuir.8b00807
Langmuir 2018, 34, 5696−5702

provide a clear description of the molecular adsorption geometry.

EXPERIMENTAL SECTION

Materials. Photoelectron spectroscopy and NEXAFS measurements were carried out using an Au(111) single crystal (MaTecK GmbH). 6-MP was purchased from Sigma-Aldrich and used as received. Absolute ethanol of analytical grade was used to prepare solutions.

Sample Preparation. The Au(111) crystal was Ar^+-sputtered and annealed, until no impurities were detected by X-ray photoelectron spectroscopy (XPS). SAM formation was performed under an ultrapure Ar atmosphere in a ultrahigh vacuum (UHV) chamber equipped with a transfer system that allows transferring the Au(111) sample between UHV and the atmospheric liquid reactor attached to the UHV chamber (described fully elsewhere).[14] The clean Au crystal was placed in contact with a 1 mM solution of 6-MP in ethanol at room temperature overnight. This was followed by copious rinsing with ethanol and drying with an Ar stream. Afterward, the functionalized surface was transferred back to the UHV analysis chamber. Note that we tried varying the molecular coverage by changing the immersion time from 30 min to 24 h, observing the same coverage in all cases.

Photoelectron Spectroscopies. XPS measurements were performed using an UHV chamber (base pressure 5×10^{-10} mbar) with a SPECS spectrometer system equipped with a 150 mm mean radius hemispherical electron energy analyzer and a nine Channeltron detector. XP spectra were acquired at a constant pass energy of 20 eV using a monochromatic Al Kα (1486.6 eV) source operated at 15 kV and 20 mA at a detection angle of 20° with respect to the sample normal. Binding energies are referred to the Au $4f_{7/2}$ emission at 84 eV. Ultraviolet photoelectron spectroscopy (UPS) spectra were acquired using a He I radiation source (21.21 eV) with normal detection, using a constant pass energy of 2 eV. Samples were biased −10 V to resolve the secondary electron cutoff in the UPS spectra. Work function values were determined from the width of the UPS spectra, as discussed below.

NEXAFS. NEXAFS measurements were carried out at the Brazilian synchrotron light source (LNLS), Campinas, Brazil using the planar grating monochromator beamline for soft X-ray spectroscopy (100−1500 eV) as the monochromatic photon source. Experiments were performed using the photoemission end station with a base pressure of 10^{-10} mbar. NEXAFS spectra were obtained by measuring the total electron yield (electron current at the sample) simultaneously with a photon flux monitor (electron current at an Au mesh). The final data were normalized with respect to the Au mesh electron current to correct for fluctuations in the beam intensity. NEXAFS spectra were recorded at 90°, 70°, 50°, and 30° photon incidence angles with respect to the sample surface. All angle-dependent geometry effects (e.g., sampling a different number of surface species) were eliminated by normalizing the resonant intensities to the angle-independent K-edge jump in all spectra.[15]

STM. STM imaging was done in air in the constant current mode with a Nanoscope IIIa microscope from Veeco Instruments (Santa Barbara, CA) with mechanically cut Pt−Ir tips (80:20%, Goodfellow, UK). Typical tunneling currents, bias voltages, and scan rates were 0.3−0.5 nA, 200−500 mV, and 1−5 Hz, respectively. Evaporated Au films on glass with (111) preferred orientation (AF 45 Berliner Glass KG, Germany) were used as substrates. After annealing for 5 min using a hydrogen flame, the Au substrates exhibit atomically smooth (111) terraces (usually 100−500 nm wide) separated by monatomic high steps.

Computational Methods. Electronic structure calculations were performed using DFT with the periodic plane-wave basis set code VASP 5.2.12.[16] We have followed the scheme of nonlocal functional proposed by Dion et al.,[17] vdW-DF, and the optimized Becke88 exchange functional, optB88-vdW,[18] to take into account van der Waals (vdW) interactions. The projector augmented plane wave method has been used to represent the atomic cores with the Perdew−Burke−Ernzerhof potential.[19] The electronic wave functions were expanded in a plane-wave basis set with a 420 eV cutoff energy. Optimal grid of Monkhorst−Pack[20] k-points $7 \times 3 \times 1$ has been used for numerical integration in the reciprocal space of the $\begin{pmatrix} 2 & 0 \\ 3 & 6 \end{pmatrix}$ unit cell. The Au(111)-(1×1) substrates were represented by a five atomic layer and a vacuum of ∼17 Å that separates two successive slabs. Surface relaxation is allowed in the three uppermost Au layers of the slab, and the atomic coordinates of the adsorbed species were allowed to relax without further constraints. The atomic positions were relaxed until the force on the unconstrained atoms was less than 0.03 eV $Å^{-1}$. Two 6MP radicals (without the H atom on the −SH group) per unit cell were placed just on one side of the slab, and all calculations include a dipole correction. Radical 6MP species were optimized in an asymmetric box of 20 Å × 20 Å × 40 Å dimensions.

RESULTS AND DISCUSSION

Figure 1a−d shows the C 1s, N 1s, S 2p, and Au 4f XPS spectra corresponding to the initial Au(111) surface (bottom spectra) and the 6MP-modified surface (top spectra). Initially there is no C, S, or N present on the surface, and only Au-related signals are observed. After formation of the 6MP SAM, XPS

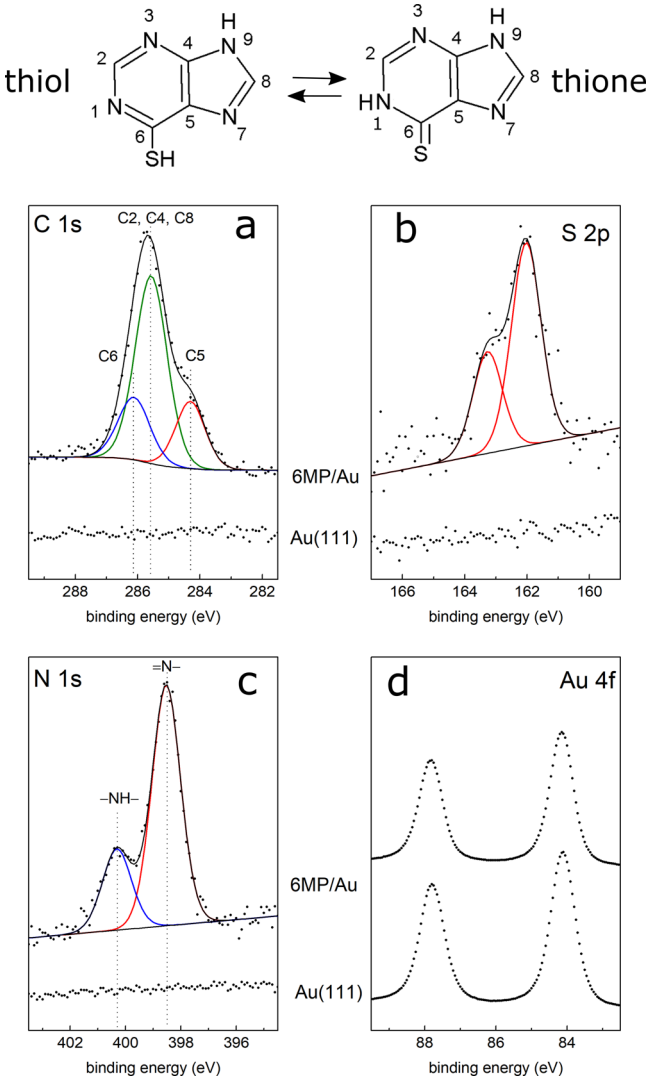

Figure 1. XPS spectra of the initial and of the 6MP-modified Au(111) surface: (a) C 1s, (b) S 2p, (c) N 1s, and (d) Au 4f. Top: Thiol and thione 6MP tautomers.

DOI: 10.1021/acs.langmuir.8b00807
Langmuir 2018, 34, 5696−5702

shows the expected presence of C, N, and S on the surface as well as the attenuation of the Au signal. The corrected XPS C/N/S ratio is 5.3:4.1:1, which is in very good agreement with the expected 5:4:1 stoichiometric ratio (see Figure 1 top). The C 1s spectrum shown in Figure 1a could be fitted with three components positioned at 284.2, 285.5, and 286.0 eV. The relative area of the peaks is 1:3:1 in excellent agreement with the assignment of Boland and Ratner:[7] the 284.2 eV component is due to C5, the 285.5 eV component is due to C2, C4, and C8, and the 286 eV component is due to C6.[7,21] The S 2p XPS region corresponding to the 6MP SAM displayed in Figure 1b shows the characteristic doublet with the S $2p_{3/2}$ at ~162 eV and the S $2p_{1/2}$ at 163.3 eV with the expected 2:1 intensity ratio.[22] The binding energy values indicate formation of thiolate S−Au bonds and the absence of thione or thiol groups on the surface,[23] that is, all S atoms on the molecule form a thiolate bond with Au.

The N 1s spectrum of 6MP SAMs requires further considerations. 6MP has several possible thione (S═C−)/thiol (HS−C−) tautomeric configurations that differ in the number of iminic (═N−) and aminic (−NH−) nitrogens.[24,25] In the thione tautomer, the molecules have two aminic and two iminic nitrogens, whereas in the thiol tautomer, the molecules have one aminic and three iminic nitrogens (Figure 1 top). Consequently, the N 1s XPS spectrum shown in Figure 1c contains two contributions: the low binding energy component at 398.4 eV is due to iminic nitrogens, whereas the high binding energy component at 400.2 eV is due to aminic nitrogens.[26] In agreement with Boland and Ratner,[7] we observe a 3:1 ratio between the iminic and aminic N components. This suggests that the molecule is adsorbed in the thiol form with three iminic and one aminic nitrogens. Our DFT calculations indicate that one of the iminic nitrogens interacts with Au, however, we do not expect this interaction to shift the N 1s binding energy position, as SAMs with amine head and anchor groups have very similar N 1s binding energies.[27−29] Thus, our XPS measurements suggest that the molecule binds in the thiol form, with three iminic nitrogens and one aminic nitrogen, ruling out the possible mixture of tautomers in the 6MP SAM under the conditions we employed for the formation of the monolayer.

The Au 4f spectra in Figure 1d show the characteristic Au $4f_{7/2}$ (84.0 eV) and Au $4f_{5/2}$ (87.7 eV) doublet with a 4:3 intensity ratio. The thickness (d) of the 6MP SAM can be estimated using the following equation: $I = I_0 \exp(-d/\lambda \cos\theta)$, where I is the substrate intensity of the SAM-covered surface and I_0 is that of the bare substrate, θ is the angle of detection with respect to the surface normal, and λ is the photoelectron attenuation length (λ is equal to 42 Å for electrons with 1402 eV kinetic energy and self-assembled alkane chains).[30] The estimated thickness is approximately 0.6 nm, suggesting a monolayer of upright standing molecules. Finally, we can use the S/Au ratio to estimate the molecular coverage in the SAM.[6] This yields a coverage of 0.25 6MP molecules per Au surface atom (3.5×10^{14} molecules cm^{-2}), which is in excellent agreement with estimations based on the electrochemical reductive desorption of 6MP SAMs on Au(111).[6]

The adsorption geometry of 6MP over Au(111) was determined using NEXAFS. Figure 2a shows the adsorption step-edge normalized N K-edge NEXAFS spectra measured at 90°, 70°, 50°, and 30° photon incidence angles with respect to the sample surface. The spectra display two main resonances: a N 1s to π^* transition at 398.7 eV[31] and a N 1s to σ^* transition

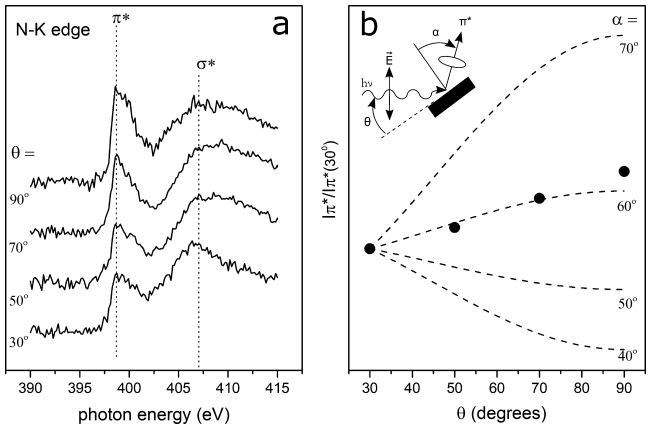

Figure 2. (a) N K-edge NEXAFS spectra taken from 6MP SAM on Au(111) as a function of the photon incidence angle. (b) Normalized N 1s to π^* transition intensity as a function of the photon incidence angle. Also shown are the theoretical curves corresponding to a π system on a threefold symmetry substrate (dashed lines).

at 407.1 eV.[12] Note that the π^* resonance is attenuated probably due to intermolecular interactions or interactions with the substrate.[32,33] The N 1s to π^* transition is larger for normal incidence, whereas the N 1s to σ^* transition is larger for grazing incidence. The observed normalized transition intensity dependence with the photon incidence angle (θ) shown in Figure 2b indicates a tilted molecular plane, in line with the dipole selection rules.[15] Figure 2b also shows the calculated normalized π^* curves for different angles between the vector π^* orbital and the surface normal (α).[15] Comparison of the experimental and calculated intensities as a function of the photon incidence angle indicates a tilt angle between the molecular plane and the surface of 61°, in line with the proposed vertical adsorption geometry on Au surfaces.[13]

The electronic structure of the 6MP SAM on Au(111) was studied using UPS. Figure 3 shows the UPS spectra corresponding to the bare Au(111) surface (red curve) and the 6MP SAM on Au(111) (black). Figure 3a shows the

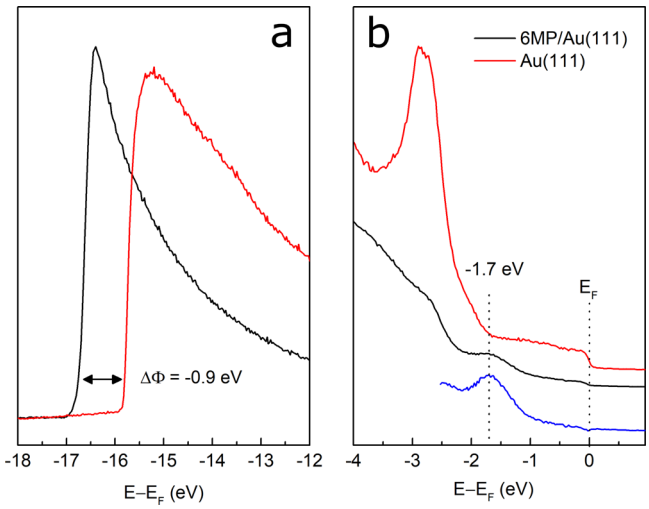

Figure 3. UPS spectra of the bare Au(111) substrate (red) and 6MP SAM on Au(111) (black). (a) shows work function changes ($\Delta\Phi$) calculated from the secondary electron cutoff and (b) shows the occupied states. Molecular states are highlighted in the 6MP/Au(111) minus the Au(111) blue spectrum.

DOI: 10.1021/acs.langmuir.8b00807
Langmuir 2018, 34, 5696−5702

secondary electron cutoff, and Figure 3b shows the occupied DOS below the Fermi edge. The UPS spectrum corresponding to the Au(111) surface shows the well-known electronic structure with a broad and flat 6s band below the Fermi edge and the intense 5d band showing one of the peaks at 2.84 eV.[34] From the width (W) of the UPS spectrum, we can calculate the work function (Φ) of our Au(111) substrate: Φ = 21.21 eV − W = 5.35 eV, which is in excellent agreement with values reported for this crystalline surface.[35]

The secondary electron cutoff shift observed in Figure 3a implies that formation of the 6MP SAM decreases the work function of Au(111) by −0.9 eV in agreement with the DFT calculations discussed below. Thus, 6MP molecules form a dipole layer with negative charges at the SAM/metal interface and positive charges at the vacuum/SAM interface.[36,37] We estimated a component of the molecular dipole perpendicular to the surface[38] equal to 1.05 D from the work function change, using a surface density of 3.47 nm^{-2} and a relative dielectric constant of the SAM equal to 1.5.[39]

When the 6MP monolayer is present on the Au(111) surface, the Au 5d and 6s bands decrease in intensity as the adsorbate attenuates the photoelectrons. Moreover, a new electronic state is observed at −1.7 eV below the Fermi edge, which can be clearly seen when the Au(111) spectrum is subtracted from the 6MP spectrum (blue curve). No electronic states are typically observed in the region up to −1.5 eV below the Fermi edge in the UPS spectra of C_2−C_{18} alkanethiol SAMs.[34,40,41] However, Alloway et al. found a very weak UPS band at −1.4 eV after formation of a C_3 alkanethiol SAM on Au(111). This state was attributed to ionization of the S−Au orbital.[42] Furthermore, benzenethiol SAMs on Au(111) also show a very weak UPS band at −1.4 eV attributed to photoemission from a S−Au orbital.[43] In line with the above, our DFT calculations discussed below indicate that 6MP on Au(111) has a very weak electronic state at round −1.2 eV below the Fermi level, which is due to the S−Au bond. Thus, the newly observed electronic state for 6MP on Au(111) at −1.7 eV cannot be attributed to photoemission from the S−Au orbital.

DFT calculations were carried out to analyze the electronic properties of the 6MP SAM on Au(111) and to gain molecular insight into the experimental results. The surface structure was modeled with a $\begin{pmatrix} 2 & 0 \\ 3 & 6 \end{pmatrix}$ unit cell, $(2 \times 3\sqrt{3})$ in Wood notation, based on the short-range ordered structure observed in the STM results discussed below (see Figure 8). The optimized structure is presented in Figure 4. It contains two 6MP moieties per unit cell, which corresponds to a surface coverage of 0.17 per unit cell (2.2×10^{14} molecules cm^{-2}). For this coverage, we found that each 6MP molecular plane in the unit cell is tilted 34.8° and 27.4° with respect to the Au surface, that is, a lower tilt angle than that estimated by NEXAFS (61°). A likely reason for this discrepancy will be presented below when discussing the STM results. The total thickness of the SAM resulting from the structure relaxation is nearly 0.3 nm, that is, smaller than that calculated from XPS measurements (0.6 nm). This difference will also be discussed below. The optimized molecular structure calculated with DFT involves a thiolate (S−Au) bond and a bond between an iminic nitrogen (=N7−) and an Au surface atom, in line with the XPS observed 3:1 iminic/aminic ratio, which rules out other adsorbed thione tautomers.

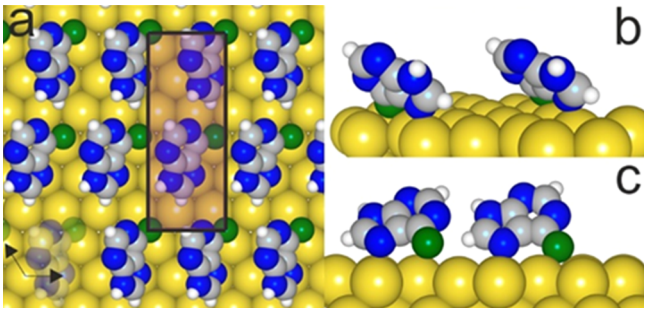

Figure 4. Optimized structure of the $\begin{pmatrix} 2 & 0 \\ 3 & 6 \end{pmatrix}$ lattice on the unreconstructed Au(111) surface with two 6MP molecules per unit cell: (a) top view; (b,c) lateral view. Color of the atoms: yellow, Au; green, S; gray, C; blue, N; white, H. The unit cell is outlined.

The difference between the DFT calculated potential in the vacuum region and the Fermi level can be used to estimate the work function.[35] Indeed, our DFT calculations yield an Au(111) work function of 5.4 eV in excellent accordance with our UPS measurement (5.35 eV). Formation of the 6MP SAM changes the potential in the direction perpendicular to the surface, yielding a work function value of 4.7 eV (Figure 5).

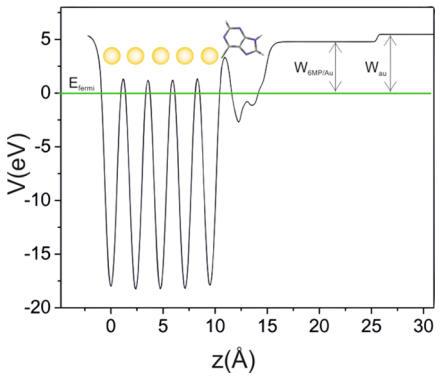

Figure 5. Plane-averaged electrostatic potential of a slab comprising five layers of Au atoms and one layer of 6MP. The Fermi energy level (E_F = 0) is indicated by a green line. The work function of the clean and the adsorbed surfaces are indicated with respect to E_F.

Therefore, the shift with respect to the clean surface is −0.7 eV. This result is in good agreement with the shift obtained from our UPS data (−0.9 eV). The smaller shift found in the calculations, by about −0.2 eV, may be related to the fact that the surface coverage modeled with DFT was 30% smaller than in the experimental measurements. As discussed above, from the estimated work function change, we can calculate the component of the molecular dipole perpendicular to the surface resulting in a value equal to $\mu_\perp$ = 1.12 D.

Figure 6a depicts the total DOS for the clean Au(111) surface and the DOS of 6MP molecules in the gas phase (in this case the energy level of the HOMO is set at 0 eV). The main features observed in the clean Au(111) DOS are a broad and flat signal below the Fermi edge that corresponds to the 6s band, followed by a sharper signal that corresponds to the 5d states. These features are in general agreement with the UPS spectrum of the clean surface presented in Figure 3. Figure 6b shows the total DOS after formation of the 6MP SAM over Au(111). Projected DOS on the S and N atoms are shown using different colors.

We also analyzed the electronic structure of the 6MP radical in the gas phase. DFT does not yield the correct HOMO−

DOI: 10.1021/acs.langmuir.8b00807
Langmuir 2018, 34, 5696−5702

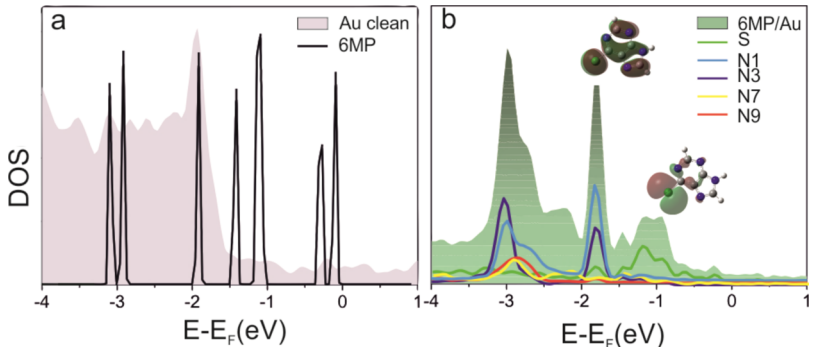

Figure 6. (a) Total DOS of Au(111) surface and 6MP molecule gas phase [the energy level of the highest occupied molecular orbital (HOMO) is set at 0 eV]. (b) 6MP adsorbed on Au(111). Projected DOS on the S and N atoms are shown in different colors.

lowest unoccupied molecular orbital (LUMO) gap (it is underestimated) nor the precise HOMO and LUMO energy location with respect to the Fermi level. However, major trends can be discussed using the shape of the frontier orbitals. After adsorption of 6MP on the Au(111) surface, the electronic states can be stabilized and shifted to lower energies. Keep in mind that after breaking the S−H bond, the highest molecular orbital is single occupied and can accept charge from the Au surface. We have determined the surface plots of the 6MP radical frontier orbitals (insets in Figure 6b). The highest charge density in this orbital is on the S atom and has the correct shape to interact with the broad Au s band, giving a hybridized electronic state at around −1.2 eV below the Fermi level. This fact is in excellent agreement with previous UPS measurements of alkyl and aromatic thiol SAMs.[42−44] Here, we should note that this band is too weak to be observed in our UPS spectrum.

It is also clear in Figure 6b that a new sharp band appears at around −1.7 eV in excellent agreement with the UPS spectrum shown in Figure 3. Its narrow shape suggests a strongly localized state. This state can be correlated with the HOMO − 1 state of the 6MP radical, which has a charge density of π character and is delocalized in the bicyclic system. The projected DOS shows that the major electronic contribution to this band comes from the pyrimidine ring. This is clearly seen in Figure 7 which shows the DOS integrated between

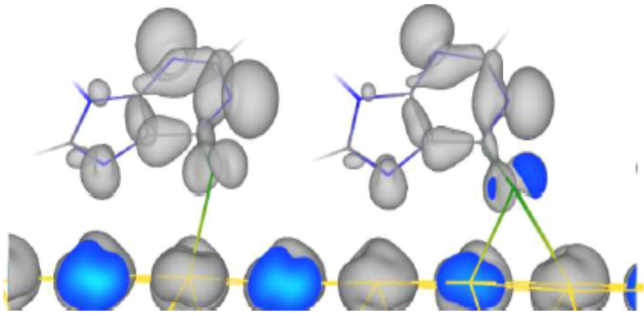

Figure 7. Charge density isosurfaces integrated between −1.6 and −2 eV for both 6MP molecules in the unit cell tilted 34.8° and 27.4° with respect to the Au surface.

−1.6 and −2 eV, with larger charge densities in the pyrimidine ring N1 and N3 nitrogens. On the other hand, the iminic nitrogen involved in the N−Au bond (N7) is strongly stabilized at −3 eV and is hybridized with the Au 5d band. Finally, we expect a weak electronic coupling of the π electrons of the 6MP aromatic structure to the metal substrate because of its adsorption geometry.

The electronic structure of the 6MP monolayer on Au(111) calculated with DFT agrees very well with that measured experimentally both in terms of the dipole layer formed and the valence band structure. Furthermore, the molecular structure calculated with DFT is in line with the photoemission data predicting a thiolate bond and an iminic nitrogen bond with the Au(111) surface. However, DFT predicts an average tilt angle of 31.1° between the molecular plane and the Au surface, whereas NEXAFS estimates a 60° tilt angle. To understand this discrepancy, we carry out STM measurements of the 6MP SAM on Au(111).

Figure 8a shows a large-area STM image corresponding to a 6MP SAM on Au(111). The surface coverage is 0.25 6MP

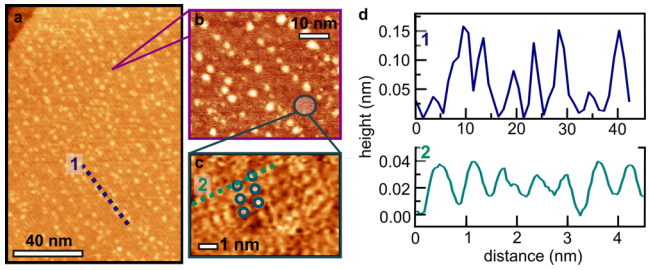

Figure 8. (a) STM image corresponding to 6MP SAM on Au(111). (b,c) Zoom-in of image (a) showing the two 6MP structures on the surface: (b) agglomerates and (c) 2D lattice. Molecule positions in the lattice are indicated as blue dots. (d) Cross-sections of the lines 1 and 2 indicated in the images.

molecules per Au surface atom, that is, the same coverage employed in the photoemission experiments discussed above. Smaller size images (Figure 8b,c) reveal that there are two distinctive regions on the surface: aligned bright spots (islands) coexisting with short-range well-ordered molecular structures. Figure 8c shows the short-range well-ordered rectangular lattice present in the regions not covered by the aligned 6MP islands. The lattice has a $\begin{pmatrix} 2 & 0 \\ 3 & 6 \end{pmatrix}$ structure, as previously determined.[6,9] Line cross-sections of the aligned 6MP islands shown in Figure 8a and the well-ordered molecular structures shown in Figure 8c indicate that the apparent height of the former is at least three times as large. Given that our DFT calculations indicate that the 6MP molecules form an average angle of 31.1° with respect to the surface in the well-ordered molecular structures, the larger apparent height of the aligned islands suggest that

DOI: 10.1021/acs.langmuir.8b00807
Langmuir 2018, 34, 5696−5702

they are composed of standing upright 6MP molecules, which are presumably interacting via $\pi-\pi$ stacking. Note that the higher 6MP islands could be interacting with Au adatoms. Recall that in our DFT model, the 6MP surface coverage is around 30% smaller than the experimental surface coverage. In a denser monolayer, the π molecular rings would tend to stand upright to accommodate more molecules. Note that the transition from flat lying to upright standing that takes place while increasing the molecular coverage has been observed for other aromatic molecules.[45] Thus, the molecular aggregates observed with STM account for the different tilt angle estimations obtained from NEXAFS measurements and DFT calculations. NEXAFS suggests a larger tilt angle, as we observe the average between the standing upright molecules in the islands and the flatter molecules in the well-ordered structures. Consequently, the experimentally estimated monolayer thickness is larger than the DFT-calculated thickness.

CONCLUSIONS

Photoemission measurements and DFT calculations show that 6MP molecules self-assemble on Au(111) bonding to the substrate via S−Au thiolate and iminic N−Au bonds. The molecule binds to the metal surface in the thiol form with three iminic and one aminic nitrogens. The SAM forms a dipole layer, with negative charges residing at the metal/monolayer interface and positive charges at the monolayer/vacuum interface. This results in a work function decrease of −0.9/−0.7 eV with respect to that of a clean Au(111) surface, depending on the surface coverage. DFT calculations show that the S−Au bond has a weak band in the total DOS located −1.2 eV below the Fermi edge, whereas the iminic nitrogen involved in bonding is stabilized at −3 eV and is hybridized with the Au 5d band. Photoemission measurements show the presence of a new electronic state located at −1.7 eV that corresponds to a π-localized molecular state with major electronic contributions in the pyrimidine ring. STM measurements show that the dense 6MP monolayers exhibit two molecular domains. The first one corresponds to short-range well-ordered molecular structures, where DFT estimates a 31° average angle between the 6MP molecular plane and the surface plane, whereas the second domain consists of aligned 6MP islands. Height profiles suggest that 6MP molecules in the latter domain are upright standing presumably interacting via $\pi-\pi$ stacking. The coexistence of both molecular structures is in agreement with the 61° adsorption angle between the molecular plane and the substrate, estimated from the NEXAFS measurements. Our results provide new physical insight into the molecular and electronic structures of SAMs bound to gold surfaces with two surface anchors.

AUTHOR INFORMATION

Corresponding Author

*E-mail: fwilliams@qi.fcen.uba.ar.

ORCID

Pilar Carro: 0000-0001-8073-9857
Roberto Salvarezza: 0000-0002-7617-4539
Federico J. Williams: 0000-0002-6194-2734

Notes

The authors declare no competing financial interest.

ACKNOWLEDGMENTS

P.C. acknowledges MINECO (ENE2016-74889-C4-2-R, AEI-FEDER-UE) and also thankfully acknowledges the computer resources provided by the Computer Support Service for Research (SAII) at the La Laguna University. R.S. thanks ANPCyT for the financial support (PICT 2016-0679). C.C.F. and F.J.W. acknowledge the financial support from CONICET. We acknowledge the financial support from the Brazilian Synchrotron Light Laboratory LNLS to use the PGM beamline.

REFERENCES

(1) Elion, G. The Purine Path to Chemotherapy. *Science* **1989**, *244*, 41−47.
(2) Karran, P.; Attard, N. Thiopurines in Current Medical Practice: Molecular Mechanisms and Contributions to Therapy-Related Cancer. *Nat. Rev. Cancer* **2008**, *8*, 24−36.
(3) Podsiadlo, P.; Sinani, V. A.; Bahng, J. H.; Kam, N. W. S.; Lee, J.; Kotov, N. A. Gold Nanoparticles Enhance the Anti-Leukemia Action of a 6-Mercaptopurine Chemotherapeutic Agent. *Langmuir* **2008**, *24*, 568−574.
(4) Ghorbani, M.; Hamishehkar, H.; Hajipour, H.; Arsalani, N.; Entezami, A. A. Ternary-Responsive Magnetic Nanocarriers for Targeted Delivery of Thiol-Containing Anticancer Drugs. *New J. Chem.* **2016**, *40*, 3561−3570.
(5) Wu, X.; Zhou, L.; Su, Y.; Dong, C.-M. Plasmonic, Targeted, and Dual Drugs-Loaded Polypeptide Composite Nanoparticles for Synergistic Cocktail Chemotherapy with Photothermal Therapy. *Biomacromolecules* **2016**, *17*, 2489−2501.
(6) Pensa, E.; Carro, P.; Rubert, A. A.; Benítez, G.; Vericat, C.; Salvarezza, R. C. Thiol with an Unusual Adsorption−Desorption Behavior: 6-Mercaptopurine on Au(111). *Langmuir* **2010**, *26*, 17068−17074.
(7) Boland, T.; Ratner, B. D. Two-Dimensional Assembly of Purines and Pyrimidines on Au(111). *Langmuir* **1994**, *10*, 3845−3852.
(8) Carro, P.; Müller, K.; Maza, F. L.; Vericat, C.; Starke, U.; Kern, K.; Salvarezza, R. C.; Grumelli, D. 6-Mercaptopurine Self-Assembled Monolayers on Gold (001)-Hex: Revealing the Fate of Gold Adatoms. *J. Phys. Chem. C* **2017**, *121*, 8938−8943.
(9) Maza, F. L.; Grumelli, D.; Carro, P.; Vericat, C.; Kern, K.; Salvarezza, R. C. The Role of the Crystalline Face in the Ordering of 6-Mercaptopurine Self-Assembled Monolayers on Gold. *Nanoscale* **2016**, *8*, 17231−17240.
(10) Bu, Y.; Huan, S.; Liu, X.; Shen, G.; Yu, R. Multiple-Angle-of-Incidence Polarization Infrared Reflection-Absorption Spectroscopy (MAI-PIRRAS) for Investigation of 6-Mercaptopurine SAMs on Smooth Silver Surface. *Vib. Spectrosc.* **2009**, *49*, 38−42.
(11) Chu, H.; Yang, H.; Huan, S.; Shen, G.; Yu, R. Orientation of 6-Mercaptopurine SAMs at the Silver Electrode as Studied by Raman Mapping and in Situ SERS. *J. Phys. Chem. B* **2006**, *110*, 5490−5497.
(12) Kim, K.-j.; Han, Y.; Zhu, J.; Baik, J.; Shin, H.; Lee, H.; Kim, B. Purine on Graphene: PES and NEXAFS Study of a Heterocyclic Aromatic Organic Compound. *Curr. Appl. Phys.* **2016**, *16*, 1120−1123.
(13) Yang, H.; Liu, Y.; Liu, Z.; Yang, Y.; Jiang, J.; Zhang, Z.; Shen, G.; Yu, R. Raman Mapping and In Situ SERS Spectroelectrochemical Studies of 6-Mercaptopurine SAMs on the Gold Electrode. *J. Phys. Chem. B* **2005**, *109*, 2739−2744.
(14) De Leo, L. P. M.; de la Llave, E.; Scherlis, D.; Williams, F. J. Molecular and Electronic Structure of Electroactive Self-Assembled Monolayers. *J. Chem. Phys.* **2013**, *138*, 114707.
(15) Stöhr, J.; Outka, D. A. Determination of Molecular Orientations on Surfaces from the Angular Dependence of near-Edge X-Ray-Absorption Fine-Structure Spectra. *Phys. Rev. B: Condens. Matter Mater. Phys.* **1987**, *36*, 7891−7905.
(16) Kresse, G.; Furthmüller, J. Efficiency of Ab-Initio Total Energy Calculations for Metals and Semiconductors Using a Plane-Wave Basis Set. *Comput. Mater. Sci.* **1996**, *6*, 15−50.

DOI: 10.1021/acs.langmuir.8b00807
Langmuir 2018, 34, 5696−5702

(17) Dion, M.; Rydberg, H.; Schröder, E.; Langreth, D. C.; Lundqvist, B. I. Van Der Waals Density Functional for General Geometries. *Phys. Rev. Lett.* **2004**, *92*, 246401.
(18) Klimeš, J.; Bowler, D. R.; Michaelides, A. Chemical Accuracy for the van Der Waals Density Functional. *J. Phys.: Condens. Matter* **2010**, *22*, 022201.
(19) Blöchl, P. E. Projector Augmented-Wave Method. *Phys. Rev. B: Condens. Matter Mater. Phys.* **1994**, *50*, 17953−17979.
(20) Monkhorst, H. J.; Pack, J. D. Special Points for Brillouin-Zone Integrations. *Phys. Rev. B: Solid State* **1976**, *13*, 5188−5192.
(21) Bolognesi, P.; O'Keeffe, P.; Feyer, V.; Plekan, O.; Prince, K.; Coreno, M.; Mattioli, G.; Bonapasta, A. A.; Zhang, W.; Carravetta, V.; Ovcharenko, Y.; Avaldi, L. Inner Shell Excitation, Ionization and Fragmentation of Pyrimidine. *J. Phys.: Conf. Ser.* **2010**, *212*, 012002.
(22) Zharnikov, M. High-Resolution X-Ray Photoelectron Spectroscopy in Studies of Self-Assembled Organic Monolayers. *J. Electron Spectrosc. Relat. Phenom.* **2010**, *178−179*, 380−393.
(23) Willey, T. M.; Vance, A. L.; van Buuren, T.; Bostedt, C.; Terminello, L. J.; Fadley, C. S. Rapid Degradation of Alkanethiol-Based Self-Assembled Monolayers on Gold in Ambient Laboratory Conditions. *Surf. Sci.* **2005**, *576*, 188−196.
(24) Viudez, A. J.; Madueño, R.; Pineda, T.; Blázquez, M. Stabilization of Gold Nanoparticles by 6-Mercaptopurine Monolayers. Effects of the Solvent Properties. *J. Phys. Chem. B* **2006**, *110*, 17840−17847.
(25) Pazderski, L.; Łakomska, I.; Wojtczak, A.; Szłyk, E.; Sitkowski, J.; Kozerski, L.; Kamieński, B.; Koźmiński, W.; Tousek, J.; Marek, R. The Studies of Tautomerism in 6-Mercaptopurine Derivatives by 1H−13C, 1H−15N NMR and 13C, 15N CPMAS-Experimental and Quantum Chemical Approach. *J. Mol. Struct.* **2006**, *785*, 205−215.
(26) Franke, M.; Marchini, F.; Steinrück, H.-P.; Lytken, O.; Williams, F. J. Surface Porphyrins Metalate with Zn Ions from Solution. *J. Phys. Chem. Lett.* **2015**, *6*, 4845−4849.
(27) Dietrich, P. M.; Graf, N.; Gross, T.; Lippitz, A.; Krakert, S.; Schüpbach, B.; Terfort, A.; Unger, W. E. S. Amine Species on Self-Assembled Monolayers of ω-Aminothiolates on Gold as Identified by XPS and NEXAFS Spectroscopy. *Surf. Interface Anal.* **2010**, *42*, 1184−1187.
(28) Marmisollé, W. A.; Capdevila, D. A.; de la Llave, E.; Williams, F. J.; Murgida, D. H. Self-Assembled Monolayers of NH2-Terminated Thiolates: Order, PKa, and Specific Adsorption. *Langmuir* **2013**, *29*, 5351−5359.
(29) de la Llave, E.; Clarenc, R.; Schiffrin, D. J.; Williams, F. J. Organization of Alkane Amines on a Gold Surface: Structure, Surface Dipole, and Electron Transfer. *J. Phys. Chem. C* **2014**, *118*, 468−475.
(30) Laibinis, P. E.; Bain, C. D.; Whitesides, G. M. Attenuation of Photoelectrons in Monolayers of N-Alkanethiols Adsorbed on Copper, Silver, and Gold. *J. Phys. Chem.* **1991**, *95*, 7017−7021.
(31) Lin, Y.-S.; Lin, H.-R.; Liu, W.-L.; Lee, Y. T.; Tseng, C.-M.; Ni, C.-K.; Liu, C.-L.; Tsai, C.-C.; Chen, J.-L.; Hu, W.-P. Measurement and Prediction of the NEXAFS Spectra of Pyrimidine and Purine and the Dissociation Following the Core Excitation. *Chem. Phys. Lett.* **2015**, *636*, 146−153.
(32) Zubavichus, Y.; Shaporenko, A.; Korolkov, V.; Grunze, M.; Zharnikov, M. X-Ray Absorption Spectroscopy of the Nucleotide Bases at the Carbon, Nitrogen, and Oxygen K-Edges. *J. Phys. Chem. B* **2008**, *112*, 13711−13716.
(33) Abu-Husein, T.; Schuster, S.; Egger, D. A.; Kind, M.; Santowski, T.; Wiesner, A.; Chiechi, R.; Zojer, E.; Terfort, A.; Zharnikov, M. The Effects of Embedded Dipoles in Aromatic Self-Assembled Monolayers. *Adv. Funct. Mater.* **2015**, *25*, 3943−3957.
(34) Rieley, H.; Price, N. J.; White, R. G.; Blyth, R. I. R.; Robinson, A. W. A NEXAFS and UPS Study of Thiol Monolayers Self-Assembled on Gold. *Surf. Sci.* **1995**, *331−333*, 189−195.
(35) De Renzi, V.; Rousseau, R.; Marchetto, D.; Biagi, R.; Scandolo, S.; del Pennino, U. Metal Work-Function Changes Induced by Organic Adsorbates: A Combined Experimental and Theoretical Study. *Phys. Rev. Lett.* **2005**, *95*, 46804.
(36) Reiss, H. The Fermi Level and the Redox Potential. *J. Phys. Chem.* **1985**, *89*, 3783−3791.
(37) Torasso, N.; Armaleo, J. M.; Tagliazucchi, M.; Williams, F. J. Simplified Approach to Work Function Modulation in Polyelectrolyte Multilayers. *Langmuir* **2017**, *33*, 2169−2176.
(38) Cahen, D.; Naaman, R.; Vager, Z. The Cooperative Molecular Field Effect. *Adv. Funct. Mater.* **2005**, *15*, 1571−1578.
(39) Romaner, L.; Heimel, G.; Ambrosch-Draxl, C.; Zojer, E. The Dielectric Constant of Self-Assembled Monolayers. *Adv. Funct. Mater.* **2008**, *18*, 3999−4006.
(40) Duwez, A.-S.; Pfister-Guillouzo, G.; Delhalle, J.; Riga, J. Probing Organization and Structural Characteristics of Alkanethiols Adsorbed on Gold and of Model Alkane Compounds through Their Valence Electronic Structure: An Ultraviolet Photoelectron Spectroscopy Study. *J. Phys. Chem. B* **2000**, *104*, 9029−9037.
(41) Duwez, A.-S. Exploiting Electron Spectroscopies to Probe the Structure and Organization of Self-Assembled Monolayers: A Review. *J. Electron Spectrosc. Relat. Phenom.* **2004**, *134*, 97−138.
(42) Alloway, D. M.; Hofmann, M.; Smith, D. L.; Gruhn, N. E.; Graham, A. L.; Colorado, R.; Wysocki, V. H.; Lee, T. R.; Lee, P. A.; Armstrong, N. R. Interface Dipoles Arising from Self-Assembled Monolayers on Gold: UV-Photoemission Studies of Alkanethiols and Partially Fluorinated Alkanethiols. *J. Phys. Chem. B* **2003**, *107*, 11690−11699.
(43) Whelan, C. M.; Barnes, C. J.; Walker, C. G. H.; Brown, N. M. D. Benzenethiol Adsorption on Au(111) Studied by Synchrotron ARUPS, HREELS and XPS. *Surf. Sci.* **1999**, *425*, 195−211.
(44) Koslowski, B.; Tschetschetkin, A.; Maurer, N.; Ziemann, P. 4-Mercaptopyridine on Au(111): A Scanning Tunneling Microscopy and Spectroscopy Study. *Phys. Chem. Chem. Phys.* **2011**, *13*, 4045.
(45) Wechsler, D.; Fernández, C. C.; Steinrück, H.-P.; Lytken, O.; Williams, F. J. Covalent Anchoring and Interfacial Reactions of Adsorbed Porphyrins on Rutile TiO2(110). *J. Phys. Chem. C* **2018**, *122*, 4480−4487.

DOI: 10.1021/acs.langmuir.8b00807
Langmuir 2018, 34, 5696−5702